COBEM 2021 26th International Congress of Mechanical Engineering
November 22-26, 2021, Virtual Congress, Brazil

COB-2021-1000
CFD SIMULATION OF FLOATING–BODY DYNAMICS FOR ENERGY CONVERSION USING OPENFOAM

Ernane Silva
Nicollas Barauce Freitas
Samuel Nobre Chaves Gonçalves
Thiago Pontin Tancredi
Filipe Dutra da Silva
André Luís Condino Fujarra
TEG Thermofluids Engineering Group, Universidade Federal de Santa Catarina, 89219600, Joinville, SC, Brazil
ernane.silva@teg.ufsc.br (corresponding author)

Abstract. *Recent studies show that the global electric energy demand must double until 2050 due to the increase of domestic consumption and the electrification of vehicles. In order to support that, and considering the need to reduce greenhouse gas emissions, the exploration of renewable energy sources has increased considerably and it is expected that by 2035 half of the global electric energy consumption will come from renewable sources. The extraction of energy from the movement of ocean waves has the highest energy density among all renewable energy sources. However, wave energy generation is still not as widely spreaded as its solar and wind counterparts mainly due to cost reasons. Therefore, novel studies and developments must be sought in this field during the coming years and to advance on that design tools are of paramount importance. For instance, hydrodynamic models are required to identify optimal geometric and operational parameters of wave energy converters. In this case, Computational Fluid Dynamics (CFD) models become more common every day, providing detailed information about the physics involved. Current models can include even dynamic mesh and fluid-structure interaction, which was unthinkable a few years ago. This paper describes the application of the open-source CFD software OpenFOAM to simulate the motion of two floating bodies subjected to waves in order to design wave energy converters. With the aim of reducing computational cost, a two-dimensional domain was adopted together with static boundary conditions for wave generation and absorption. The wave generation is based on the Stokes wave theory available in the extended OpenFOAM CFD suite OlaFlow. The results show how the relative motion of the floating bodies is affected by the wave and body characteristics and allow a first estimate of the energy conversion potential. Besides, it is shown that the model is suitable for optimization purposes given its relatively low computational cost.*

Keywords: *wave energy, floating platforms, CFD, OpenFOAM*

1. INTRODUCTION

According to McKinsey & Company (2019), world electricity consumption is expected to double by 2050, driven mainly by its growing demand in homes and the electrification of transportation. In this context, and taking into account the need to reduce carbon dioxide emissions into the atmosphere, it is expected that 50% of all energy consumed in the world will come from renewable sources by 2035. Between 2015 and 2017, more than half of the increase in global electricity generation capacity came from wind and solar energy sources. Although these are currently the dominant renewable energy sources, energy generation from waves provides the highest energy density (Clément *et al*., 2002). The energy density of waves varies between 2 and 3 kW/m^2 while for wind and solar energy it varies between 0.1 and 0.2 kW/m^2 (López *et al*., 2013). The south of Brazil has a considerable potential for generating wave energy with small seasonal variations (Pecher and Kofoed, 2016), compared to countries such as Australia, New Zealand, South Africa, and Chile, pointed out among those with the greatest potential for wave energy generation (IRENA, 2014).

There is a variety of wave energy converter systems. Oscillating water column-type systems trap air inside a cavity partially filled with water. As the water level varies inside the cavity due to the movement of the waves, the air flows alternately into and out of the cavity, promoting the movement of a turbine that captures the flow's energy. Overtopping-type systems have a similar operating principle. In this case, wave motion causes water to be pushed into a reservoir above sea level. A turbine extracts energy from the water flow returning to the sea. Finally, there are the oscillating systems, which exist in different configurations and extract energy from the oscillatory movements caused by the waves. All these systems require a power converter (PTO – Power Take-Off). In oscillating water columns and overtopping types there are turbines, while in oscillating systems there are hydraulic or electromagnetic devices (Nguyen *et al*., 2020).

Currently, wave power generation is not economically competitive when compared to existing wind and solar technologies. In order to reduce installation, foundation/mooring, operation and maintenance costs, and to enable the exploitation of this important renewable energy source, wave energy converter systems have been integrated into marine structures for other purposes, such as floating wind turbines (Pérez-Collazo *et al*., 2015) , breakwaters (Mustapa *et al*., 2017; Zhao *et al*., 2019), net tanks for aquaculture (Shi *et al*., 2019), conventional offshore platforms and platform ships (Taghipour and Moan, 2008; Wang *et al*., 2018). Studies have also considered the integration of these systems with large floating platforms for the most diverse applications, such as floating port terminals, for instance (Nguyen *et al*., 2020).

While the technology related to wave energy converters develops and new designs are sought, design tools are of paramount importance. For instance, hydrodynamic models are required to identify optimal geometric and operational parameters of wave energy converters. In this case, Computational Fluid Dynamics (CFD) models become more common every day, providing detailed information about the physics involved. Current models can include even dynamic mesh and fluid-structure interaction, which was unthinkable a few years ago. In this context, this paper describes the application of the open-source CFD software OpenFOAM to simulate the motion of two floating bodies subjected to waves. A low-cost two-dimensional model with static boundary conditions is developed in order to support the design of wave energy converters.

2. NUMERICAL MODEL

2.1 Governing equations

Instead of using OpenFOAM directly, we adopted OlaFlow, which is a set of solvers and boundary conditions developed within the OpenFOAM framework to simulate fluid dynamics for coastal, marine, hydraulic, and offshore engineering (OlaFlow, 2021). It is based on the Reynolds Averaged Navier-Stokes (RANS) equations for incompressible turbulent multiphase flow, that is,

$$\nabla . \vec{u} = 0 , \tag{1}$$

$$\frac{\partial(\rho\vec{u})}{\partial t} + \nabla.(\rho\vec{u}\vec{u}) = -\nabla p + \nabla.(\upsilon\nabla\vec{u}) + \rho f_b , \tag{2}$$

where $\vec{u}$ is the velocity of the fluid, t is time, ρ is the fluid density, p is the fluid pressure, υ is the kinematic viscosity, and f_b is the external force that may be acting on the system.

Since the system is settled to be a two-phase flow, with air and water, the volume of fluid method (VoF) is used to determine the range of the fluids and their interface. Therefore, an additional transport equation (Eq. (3)) is used to compute the volume fraction α, which can have any value between 0 (air) and 1 (water).

$$\frac{\partial\alpha}{\partial t} + \nabla.(\vec{u}\alpha) + \nabla.[\vec{u}_r\alpha(1-\alpha)] = 0, \tag{3}$$

$$\vec{u}_r = min[c_r|\vec{u}|, (|\vec{u}|)\,]. \tag{4}$$

In Eq. (4) $\vec{u}_r$ stands for the compression velocity, which acts to reduce interface smearing, and c_r is a parameter that can be defined by the user, with 1 as the default value. As all other properties, the density in any point of the domain can be computed as

$$\rho = \alpha\rho_{water} + (1-\alpha)\rho_{air} . \tag{5}$$

OlaFlow adopts the PIMPLE algorithm for the pressure-velocity coupling, which is a combination of PISO (pressure-implicit with splitting of operator) and SIMPLE (semi-implicit method for pressure-linked equations) (Versteeg and Malalasekera, 2007) available in OpenFOAM. The algorithm structure is almost all based on PISO, but allows under-relaxation to certify the convergence of the equations at each time step (OlaFlow, 2021). All simulations reported in the present study were carried out assuming laminar flow since turbulent effects do not significantly change the results, as observed by Windt *et al*. (2020) in a similar study.

2.2 Computational domain and boundary conditions

The computational domain and boundary conditions are shown in Figure 1. A two-dimensional domain was adopted to reduce the computational cost, with 6.81 m in length and 1.8 m in height (Windt *et al*., 2020). Two independent rectangular floating bodies with dimensions 0.24 m x 0.22 m and 0.48 m apart from each other were placed in the middle of the domain and were allowed to translate in the vertical direction and to rotate. The density of the floating bodies was

defined as 500 kg/m^3 and the center of mass located 5 cm below the centerpoint. For the wave generation and absorption, we adopted the static boundary method, which is based on the Stokes wave theory. In this method the velocity $\vec{u}(\vec{x},t)$ and the free surface elevation $\eta(\vec{x},t)$ are defined as Dirichlet boundary conditions in both generation and absorption boundaries of the domain. Different from other methods, such as dynamic boundary conditions and relaxation zones, the static boundary method reduces the computational cost by avoiding mesh movement and the use of extended domains. At the absorption boundary, a correction velocity $\vec{u}_c(\vec{x},t)$ is generated in order to cancel possible reflected waves. This correction velocity has the same module of the incident velocity but opposite direction so as to terminate the incident waves (Windt *et al*., 2019). At the bottom of the domain and the surface of the floating bodies, a no-slip boundary condition was considered. Finally, at the top, we adopted the *pressureInletOutletVelocity* boundary condition available in OpenFOAM to represent the side of the domain open to the atmosphere. This boundary condition assigns a zero gradient condition for outflow or a prescribed velocity, calculated based on the internal-cell values, for inflow. The baseline mesh was built of 200 cells in horizontal and 70 cells in the vertical direction, constituting a total of approximately 14,000 cells. A refined region is created near the interface between air and water in order to capture the free surface elevation with accuracy. Therefore, in the vertical direction 40 cells are placed in a region with ~ 0.1 m around the centerline of the domain. The temporal discretization was varied according to the period of the wave, being defined as $T/100$. The simulations were run until a steady-state condition was reached, which was verified visually.

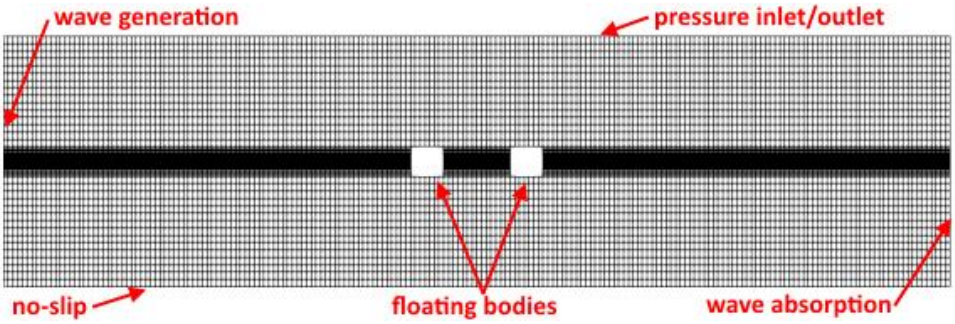

Figure 1. Computational domain and boundary conditions.

3. RESULTS AND DISCUSSION

3.1 Mesh analysis

Prior to performing the simulations with floating bodies, a mesh analysis was performed considering only the wave generation and absorption. That is, the same computational domain and boundary conditions described in Figure 1 were used, except that the two floating bodies were removed. In order to assess the mesh quality, the free surface elevation was monitored in two different positions along the centerline of the domain, namely probe A and probe B, located 0.2 m and 2.16 m, respectively, downstream of the wave generation boundary condition. Figures 2a and 2b compare the results of the coarse and fine meshes obtained for a wave with amplitude 0.115 m, wavelength 4.50 m, and period 1.84 s. The coarse mesh is the one described in the previous section while the fine mesh has twice the number of cells in each direction, making up a total of 56,000 cells.

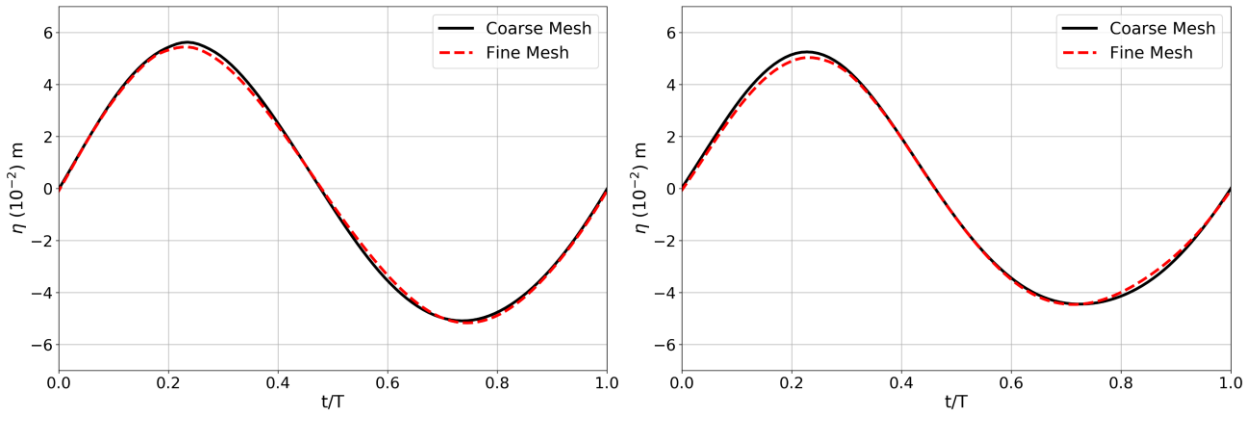

Figure 2. Free surface elevation at probes A (a) and B (b) for different mesh refinements.

The results indicate that using a finer mesh results in only minor variation in the free surface elevation at the expense of a much higher computational cost. For instance, the simulation with the coarse mesh took approximately 8 minutes while that with the fine mesh took about one hour. Therefore, we decided to perform the following analyses only with the coarse mesh since we intend to have a low-cost simulation model for future optimization studies.

3.2 **Validation of the model**

The model was validated against experimental and numerical data from Windt *et al*. (2020) for the case where there is no floating body and only wave generation and absorption are considered. Waves with different characteristics were simulated and the free surface elevation was monitored at probes A and B. Figures 3a and 3b show the results obtained for the first wave (wave 1), with amplitude 0.021 m, wavelength 1.56 m, and period 0.99 s, while Figures 3c and 3d show the results for the second wave (wave 2), with amplitude 0.115 m, wavelength 4.50 m and period 1.84 s. According to Le Méhauté (1976), both waves can be well described as second-order Stokes waves, or Stokes II.

As can be seen, the results obtained are in good agreement with those provided by Windt *et al*. (2020). Larger discrepancies in relation to the experimental data are found for the second wave as also observed by Windt *et al*. (2020). In this case, the present model underestimates the maximum amplitude of the free surface at probe A by 10.2% while the numerical model developed by the authors overestimates this parameter by 7.2%. For probe B, the present model overestimates the free surface elevation by 11.9% in comparison to 41.8% in the model of Windt *et al*. (2020). Table 1 also shows the wave amplitudes and the deviation between the present results and those from Windt *et al*. (2020). We can see that the present results are closer to the experimental data, even though both numerical models consider the same equations and boundary conditions. This may be related to slightly different settings for the boundary conditions and must be further investigated. The remaining discrepancies observed in relation to the experimental data can also be caused by wave reflection in the experimental wave tank. This hypothesis is raised due to the visible peak flatness in the experimental results of Figure 3d in relation to Figure 3c. Nevertheless, given that our numerical predictions showed reasonable accuracy for the free surface elevation in relation to experimental data, we consider the model validated for the purpose of developing a low-cost CFD model. It is important to note that the simulation of waves only took approximately 8 minutes running in a single core of a regular personal computer.

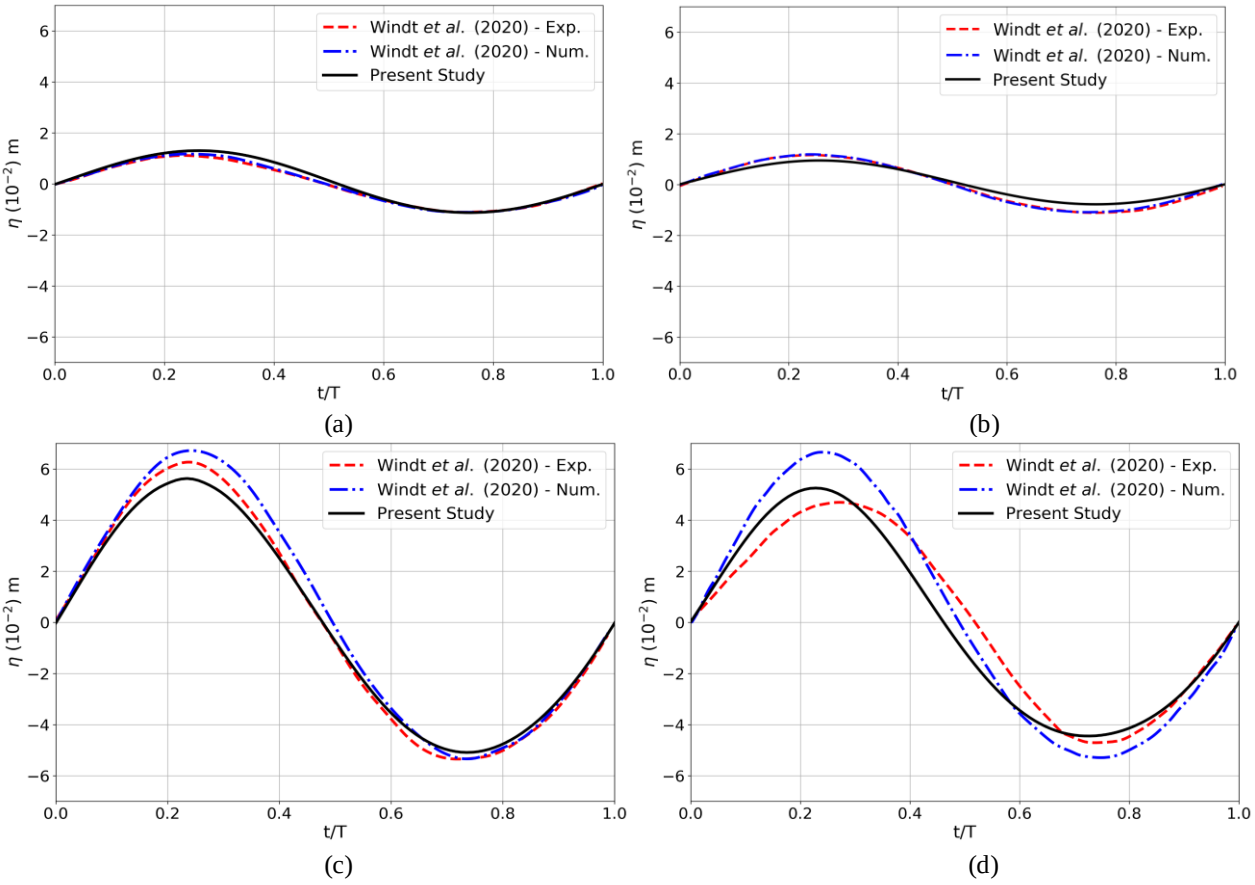

Figure 3. Free surface elevation at probes A and B for different waves. (a) wave 1 probe A, (b) wave 1 probe B, (c) wave 2 probe A, and (d) wave 2 probe B.

Table 1. Wave amplitudes and deviation relative to the present results.

Wave 1	**Probe A**	**Probe B**
Present Study	2.43	1.72
Windt *et al.* (2020) - Numeric	2.28 (- 6.2%)	2.27 (+31.9%)
Windt *et al.* (2020) - Experimental	2.23 (-8.2%)	2.27 (+31.9%)
Wave 2	**Probe A**	**Probe B**
Present Study	10.71	9.70
Windt *et al.* (2020) - Numeric	12.06 (+12.6%)	11.95 (+23.2%)
Windt *et al.* (2020) - Experimental	11.61 (+8.4%)	9.40 (-3.1%)

3.3 **Floating-body dynamics**

Figure 4 shows the vertical position of the floating objects' center of mass when subjected to waves 1 and 2. "First object" refers to the body closer to the wave generation boundary, whereas "Second object" refers to the other object. When the bodies are subjected to wave 1, the vertical displacement of the second object is reduced by the influence of the first object (Figure 4a). On the other hand, when the bodies are subjected to wave 2, the amplitude of their displacements are very similar, meaning the bodies are virtually transparent for the incident wave (Figure 4b). Besides, we can see clearly that the phase difference between the two objects is more pronounced for wave 1. This occurs since the bodies are placed approximately half wavelength apart, in the sense that when the first object is on the wave crest the second one is near the wave trough. The opposite happens for wave 2. Similar considerations can be made when the distance between the bodies is increased to 1.32 m (Figure 4c and Figure 4d). In this case, the dephasing is more evident for wave 2. The amplitudes remain roughly the same. A significant increase in computational time was observed in relation to the wave-only simulations due to the dynamic mesh. For wave 1 the simulation took approximately 2 hours while for wave 2 the simulation took approximately 4 hours. Clearly, such simulation times could be reduced considerably with parallel processing.

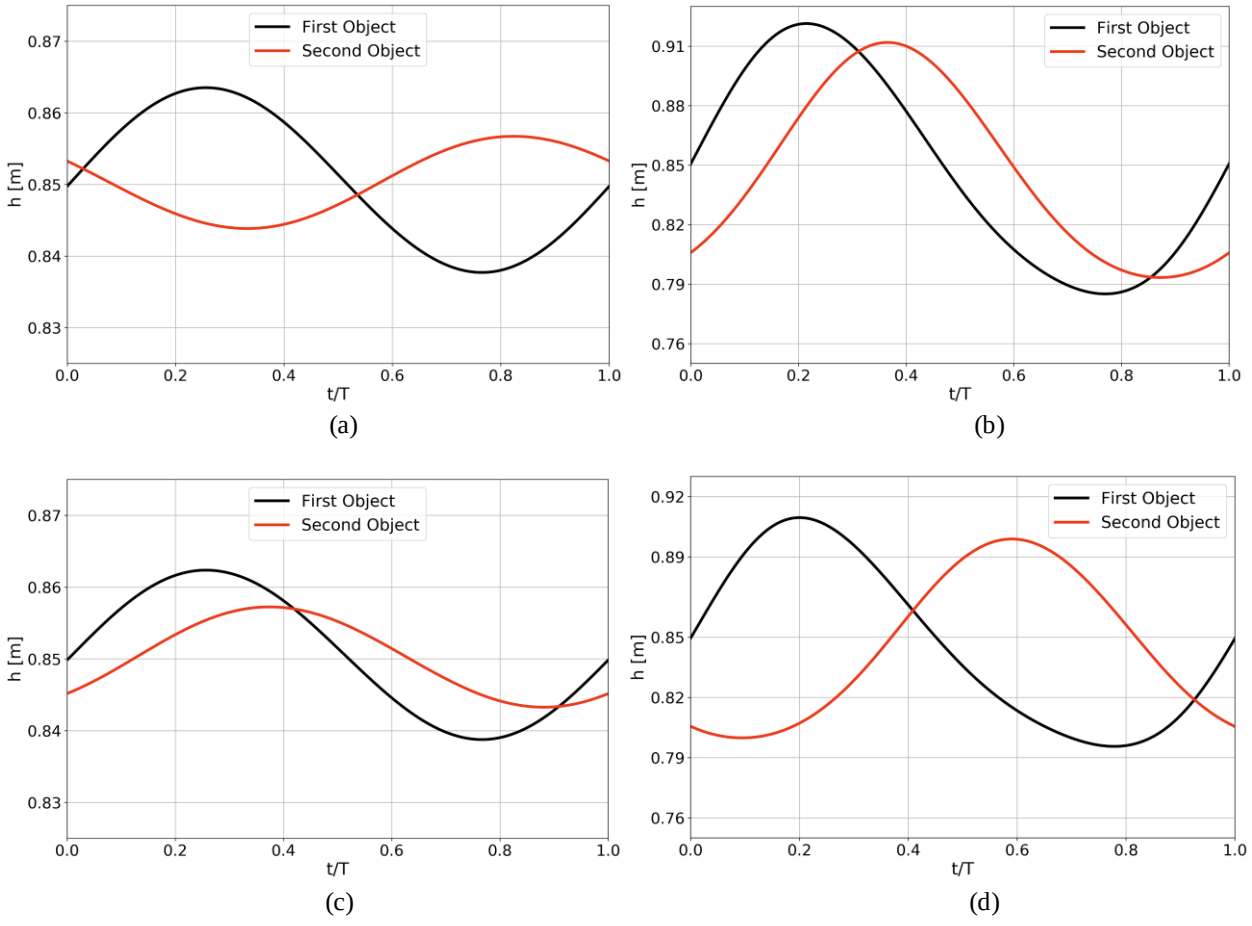

Figure 4. Vertical displacement of the floating objects' center of mass when subject to waves 1 (a) and 2 (b) for a distance between objects of 0.48 m and waves 1 (c) and 2 (d) for a distance of 1.32 m.

4. CONCLUSIONS

The present study describes the application of the open-source CFD code OpenFOAM and its extension OlaFlow to simulate the interaction between waves and floating bodies. A two-dimensional model was developed taking into account static boundary conditions for wave generation and absorption. Simulations without the floating bodies were carried out to validate the wave dynamics. The results were compared to experimental data available in the literature and we found discrepancies of around 10% for the free surface elevation, which are close to other numerical predictions in the literature. Therefore, the simulation of wave generation and absorption was considered validated for the purposes of the present study. Next, simulations were performed considering the existence of two floating bodies in the domain. Two different waves were considered and we observed how the amplitude and relative phase of the displacements are affected by the wave characteristics. The model developed constitutes a simulation tool suitable for the prediction of the hydrodynamic performance of wave energy converters. Future studies should try to improve the accuracy of the wave dynamics by adopting other boundary conditions for wave generation and absorption while keeping the low computational cost. Moreover, the model must be employed to design wave energy converters for application in specific sites along the Brazilian coast.

5. REFERENCES

Clément, A., McCullen, P., Falcão, A., Fiorentino, A., Gardner, F., Hammarlund, K., Lemonis, G., Lewis, T., Nielsen, K., Petroncini, S., Pontes, M. T., Schild, P., Sjöström, B. O., Sørensen, H. C., and Thorpe, T., 2002. "Wave energy in Europe: current status and perspectives". Renewable and Sustainable Energy Reviews, Vol. 6, No. 5, pp. 405–431.

Le Méhauté, B., 1976. Introduction to hydrodynamics and water waves. Springer-Verlag, New York, USA.

López, I., Andreu, J., Ceballos, S., De Alegría, I. M., and Kortabarria, I., 2013. "Review of wave energy technologies and the necessary power-equipment". Renewable and Sustainable Energy Reviews, Vol. 27, pp. 413–434.

IRENA, 2014, Wave energy technology brief, International Renewable Energy Agency, https://www.irena.org/publications/2014/Jun/Wave-energy. Accessed 1 June 2021.

McKinsey & Company, 2019, Global energy perspective 2019: reference case, https://www.mckinsey.com/~/media/mckinsey/industries/oil%20and%20gas/our%20insights/global%20energy%20perspective%202019/mckinsey-energy-insights-global-energy-perspective-2019_reference-case-summary.ashx. Accessed 1 June 2021.

Mustapa, M. A., Yaakob, O. B., Ahmed, Y. M., Rheem, C. K., Koh, K. K., and Adnan, F. A., 2017. "Wave energy device and breakwater integration: a review". Renewable and Sustainable Energy Reviews, Vol. 77, 43–58.

Nguyen, H. P., Wang, C. M., Tay, Z. Y., and Luong, V. H., 2020. "Wave energy converter and large floating platform integration: a review". Ocean Engineering, Vol. 213, 107768.

OlaFlow, 2021, OlaFlow website, https://olaflow.github.io/. Accessed 16 June 2021.

Pecher, A., and Kofoed, P., 2016. Handbook of ocean wave energy, 7. Ed. Springer.

Pérez-Collazo, C., Greaves, D., and Iglesias, G., 2015. "A review of combined wave and offshore wind energy". Renewable and Sustainable Energy Reviews, Vol. 42, pp. 141–153.

Shi, H., Dong, X., Feng, L., and Han, Z., 2019. "Experimental study on the hydrodynamic performance of a heaving buoy assembled on a net cage platform. Journal of Ocean University of China, Vol. 18, No. 5, pp. 1031–1040.

Taghipour, R., and Moan, T., 2008. "Efficient frequency-domain analysis of dynamic response for the multi-body wave energy converter in multi-directional wave". In Proceedings of the 18th International Offshore and Polar Engineering Conference. Vancouver, Canada.

Versteeg, H. K., and Malalasekera, W., 2007. An introduction to computational fluid dynamics: the finite volume method. Pearson Education, Essex, England.

Wang, L., Kolios, A., Cui, L., and Sheng, Q., 2018. "Flexible multibody dynamics modelling of point-absorber wave energy converters". Renewable Energy, Vol. 127, pp. 790–801.

Windt, C., Davidson, J., Schmitt, P., and Ringwood, J. V., 2019. On the assessment of numerical wave makers in CFD simulations. Journal of Marine Science and Engineering, Vol. 7, No. 2.

Windt, C., Faedo, N., García-Violini, D., Peña-Sanchez, Y., Davidson, J., Ferri, F., and Ringwood, J. V., 2020. Validation of a CFD-based numerical wave tank model of the 1/20th scale wavestar wave energy converter. Fluids, Vol. 5, No. 3.

Zhao, X. L., Ning, D. Z., Zou, Q. P., Qiao, D. S., and Cai, S. Q., 2019. "Hybrid floating breakwater-WEC system: a review". Ocean Engineering, Vol. 186, 106126.

6. RESPONSIBILITY NOTICE

The authors are the only responsible for the printed material included in this paper.